ELSEVIER

Chemical Engineering Journal 133 (2007) 157–163

Chemical Engineering Journal

www.elsevier.com/locate/cej

A silicon-based miniaturized reformer for high power electric devices

Oh Joong Kwon, Sun-Mi Hwang, In Kyu Song, Ho-In Lee, Jae Jeong Kim *

Research Center for Energy Conversion and Storage, School of Chemical and Biological Engineering, Seoul National University, Shillim-dong, Kwanak-gu, Seoul 151-742, Republic of Korea

Received 9 November 2006; received in revised form 1 February 2007; accepted 1 March 2007

Abstract

A reformer stack was made using a silicon technology and a fill-and-dry catalyst coating method. Before fabricating the reformer stack, various conditions were considered to find out an optimum operating condition. To coat a catalyst layer inside micro-channels, an Al_2O_3 layer and a SiO_2 layer were deposited and investigated as an adhesion layer. The performances of a parallel channel reformer and a serpentine channel reformer were examined to determine the effect of varying channel designs. The parallel channel reformer and the serpentine channel reformer were fabricated using a SiO_2 layer and deionized (D.I.) water-based catalyst those showed better adhesion and improved catalytic activity than the Al_2O_3 adhesion layer and than the Al_2O_3 sol-based catalyst. Based on the hydrogen production rate per unit volume of the reformer (hydrogen production rate divided by the volume of the reformer), the parallel channel reformer was superior to the serpentine channel reformer, when the performances of the two designs were compared. The parallel channel reformer yielded a hydrogen production rate of 177 $cm^3\,min^{-1}$ per unit reformer volume. Because of a high volumetric hydrogen production rate and simple fabrication process, the parallel channel reformers were used to construct a reformer stack. The hydrogen production rate of the reformer stack was 754 $cm^3\,min^{-1}$, and its volume was 15 cm^3.

Keywords: Miniaturized reformer; Reformer stack; Adhesion layer; Channel design

1. Introduction

Fuel cells have been highlighted in various areas as an energy source which can replace secondary batteries since 1990s. High energy density and eco-friendly characteristics are the issues of a future energy system and fuel cells are the energy systems which can satisfy these requirements. Thus, they have been studied extensively and have substituted into existing energy systems in recent years. An energy source for automobiles, Residual Power Generators (RPGs), plants and buildings are the areas in which fuel cells are going to be utilized. At the same time, fuel cells are extending their application areas from large systems to small systems such as micro-sensors, cellular phones, Personal Digital Assistants (PDAs), and notebook computers [1–4]. However, scaling down the application is far more difficult than scaling up, due to the necessity of miniaturizing both the fuel cell and the peripheral devices.

A fuel storing and supplying component occupies the largest volume among peripheral devices. To reduce the volume needed for the fuel storage, several methods such as a metal hydride, a chemical hydride, compressed hydrogen and a miniaturized reformer have been researched. Among them, the miniaturized reformer is considered as the fuel source with high potential for supplying hydrogen to the fuel cell, because it has high energy density and fast load response. Miniaturized reformers are made using a conventional micro-machining technology and silicon fabrication technologies [5–8]. Miniaturized reformers made using silicon fabrication technologies use different concepts compared to the conventional packed bed type reformer. They use micro-channels and layer type catalysts instead of tubular type reactors and packed bed type catalysts [9]. Micro-channel systems give many advantages to the reformer by enabling fast mass transfer and heat transfer, and silicon technologies have the advantages of simple and accurate fabrication process, integrated control system and sensors with the reactor, and small reactor volume that is obtained by applying thin film heater and direct bonding method.

Silicon fabrication technologies have been developed through semiconductor industries. The fabrication processes for miniaturized reformers employ these established technologies. A lithography, silicon wet etching, an anodic bonding and a thin

* Corresponding author. Tel.: +82 2 880 8863; fax: +82 2 888 2705.
E-mail address: jjkimm@snu.ac.kr (J.J. Kim).

1385-8947/$ – see front matter © 2007 Elsevier B.V. All rights reserved.
doi:10.1016/j.cej.2007.03.010

film deposition have been adopted from silicon technologies, and fabrication of miniaturized reformers was successfully accomplished using these technologies [10–13]. But, the amount of hydrogen supplied from a unit miniaturized reformer is too low to introduce the miniaturized reformer to high power electric devices, thus the scaling up of the miniaturized reformer is required.

To scale up the silicon-based reformer, the parallel channels are essential to reduce a pressure drop caused by high reactant and product flow rates. However, the Al_2O_3 layer, which has been used as the adhesion layer in the silicon-based reformer, restricts the channel design. To coat the Al_2O_3 layer inside of pre-assembled micro-channels, an air pushing step is necessary to remove excessive sol at the center of the channel. To remove excessive sol with the air pushing, channels of the reformer should be only in the serpentine configuration. If parallel channels are used for a reformer, many channels are blocked by the sol with the present Al_2O_3 layer coating method. Thus, new fabrication process for the adhesion layer is required to scale up the silicon-based reformers, and this paper suggests the SiO_2 layer, which can be formed by oxidizing the silicon substrate, as an adhesion layer.

This study tested the adhesion property of a SiO_2 layer and measured the catalyst activity on the SiO_2 adhesion layer. The test results were compared with results obtained from Al_2O_3 adhesion layer, and the SiO_2 layer was applied into the parallel channel reformer. After checking the performance of the parallel channel reformer, the scaling up of the silicon-based reformer was carried out with the parallel channel design. The performance of a reformer stack was focused on a hydrogen production rate and a CO concentration.

2. Fabrication

Fig. 1 shows the schematic diagram of a catalyst layer of a reformer. A Cu–ZnO–Al_2O_3 catalyst coated either on the Al_2O_3 or the SiO_2 layer was used for a methanol steam reforming reaction. Miniaturized reformer fabrication processes were exactly the same as our previous study except the SiO_2 adhesion layer and the reformer channel design [13]. (1 1 0) silicon wafers were etched with a 30 wt% KOH solution at 80 °C for 2 h. After bonding etched silicon wafers with Pyrex™, the

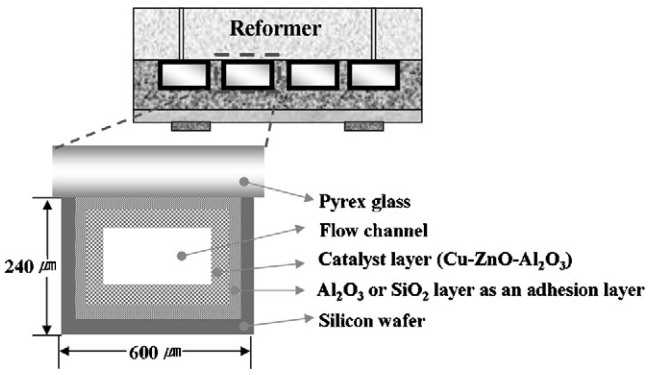

Fig. 1. A schematic diagram of a catalyst layer of a reformer.

Al_2O_3 layer or the SiO_2 layer was formed inside of the channels as an adhesion layer. The Al_2O_3 layer was formed using an Al_2O_3 slurry prepared through Yoldas process, and the SiO_2 layer was prepared by dry oxidation of the Si substrate [14]. A thin film heater composed of TaN_x (80 nm)/Ta (a few nm)/Au (300 nm) was deposited on the back of the silicon wafers by direct current (dc) magnetron sputter. Following this step, a D.I. water-based Cu–ZnO–Al_2O_3 catalyst slurry was coated by a fill-and-dry coating method, and it was calcined at 300 °C for 3 h [13]. The commercial Cu–ZnO–Al_2O_3 reforming catalyst (MDC-3, Süd-Chemie) was used in all experiments. After finishing the fabrication of a silicon-based reformer, the silicon-based reformer was packaged with stainless steel plates to analyze the performance. Fig. 2(c) and (d) shows the photo images of an as-prepared and packaged parallel channel reformer. The volume of the as-prepared parallel channel reformer and the packaged parallel channel reformer were 1.03 and 8.3 cm^3, respectively.

3. Experiment

A schematic diagram of the experimental setup is shown in Fig. 3. A methanol solution was fed by a syringe pump and the temperature of the reformer was controlled by a power supply, a relay, and a Proportional-Integrate-Derivative (PID) algorithm programmed by LabVIEW™. Product gas flow rates and compositions were measured by a digital flow meter (Optiflow 650, Agilent) and a gas chromatograph (Varian CP 4900), respectively, during the duration of the experiments.

Physical property analysis of the Al_2O_3 layer and the SiO_2 layer was carried out. After Cu–ZnO–Al_2O_3 catalysts were coated on both adhesion layers, the adhesion was measured by 3M tape test method recommend by the American Society for Testing and Materials (ASTM), and by a Field Emission Scanning Electron Microscopy (FESEM). And then, catalytic activities of Cu–ZnO–Al_2O_3 were measured on both SiO_2 adhesion layer and on Al_2O_3 adhesion layer to find out the adhesion layer effect on the performance of catalysts.

The Al_2O_3 layer coating process has restricted the channel design to the serpentine configuration, because it requires the excessive sol removal step, that is only possible when the channel is serpentine. However, with the introduction of the SiO_2 adhesion layer, reformers could have various designs by overcoming the coating process limitation. Thus, the SiO_2 layer was applied to micro-channels of the parallel channel reformer. The performance of the parallel channel reformer was compared with the result of the serpentine channel reformer and was focused on a specific hydrogen production rate and a CO concentration.

A reformer stack was fabricated with the parallel channel reformer, because it was superior to the serpentine channel reformer in the aspect of a fabrication simplicity and of a hydrogen production rate per unit volume of the reformer (hydrogen production rate divided with the volume of reformer). The hydrogen production rate and the CO concentration were measured with digital flow meter and gas chromatograph (GC), respectively.

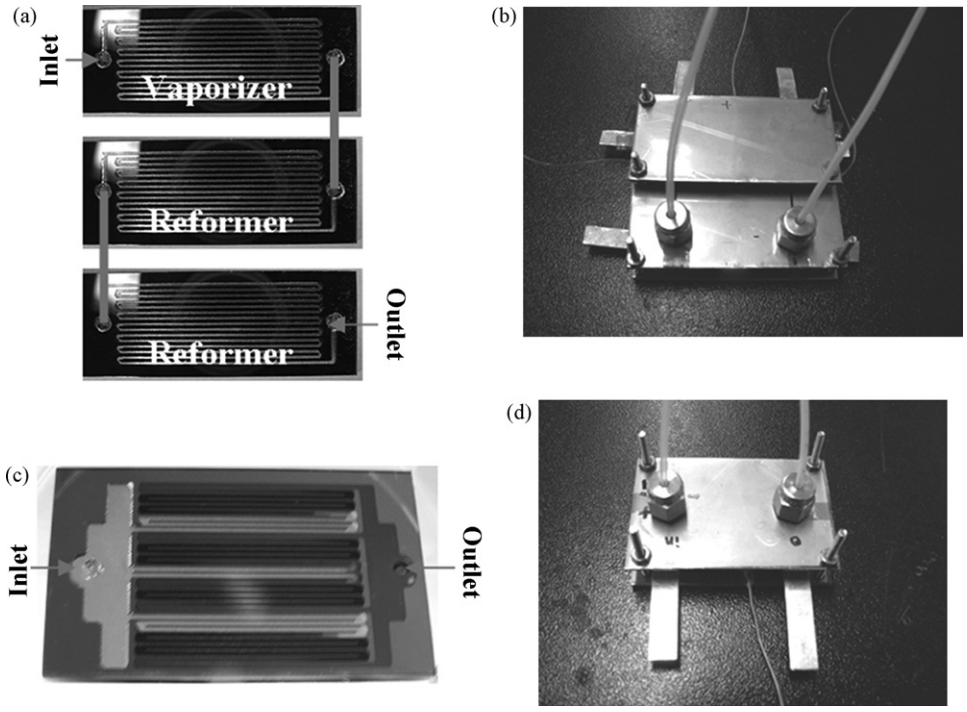

Fig. 2. (a) A schematic diagram of a serpentine channel reformer, (b) a photo image of a serpentine channel reformer packaged with stainless steel plate, (c) a photo image of a parallel channel reformer, and (d) a photo image of a parallel channel reformer packaged with stainless steel plate.

4. Results and discussion

Fig. 4(a) and (b) show the coating profiles of the adhesion layers formed inside of micro-channels. An Al_2O_3 layer was coated by a wash coating method using an Al_2O_3 sol prepared by the Yoldas process. As shown in Fig. 4(a), the thickness of the Al_2O_3 adhesion layer was 0.43 μm at the side wall and 0.37 μm at the bottom wall, respectively. On the other hand, the SiO_2 adhesion layer was formed by oxidizing a Si substrate at 300 °C, but it was not identified from a FESEM image due to the FESEM resolution limitation. Thus, XPS was used to measure the SiO_2 adhesion layer thickness. Fig. 5 shows the result of XPS data for a bare Si substrate, and Eq. (1) was applied to calculate the thickness from XPS data [15]:

$$t_{ox} = \lambda_{SiO_2} \sin\theta \ln\left\{\left[\left(\frac{1}{\beta}\right)\left(\frac{I^{exp}_{SiO_2}}{I^{exp}_{Si}}\right)\right] + 1\right\} \quad (1)$$

Each symbol means that λ_{SiO_2} = attenuation length of the Si 2p photoelectrons in SiO_2, θ = angle between the sample surface plane and the electron analyzer, $\beta = I^{\infty}_{SiO_2}/I^{\infty}_{Si}$ (the Si 2p intensity from infinitely thick SiO_2 and Si, respectively) and $I^{exp}_{SiO_2}/I^{exp}_{Si}$ = the ratio of intensities from unknown film. The angle between the sample surface plane and the electron analyzer was 90°, and the $I^{exp}_{SiO_2}/I^{exp}_{SiO_2}$ value was 1.254 in this analysis. The thickness of SiO_2 layer calculated by inserting these values into Eq. (1) (attenuation length = 2.7 nm, and β = 0.83) was 2.4 nm, which was very similar with the result obtained by theoretical calculation at 300 °C for 3 h [15,16].

Although the thicknesses of the SiO_2 layer and the Al_2O_3 layer were quite different, both adhesion layers showed good adhesion property as shown in Fig. 6(a) and (b). In both adhesion layers, the Cu–ZnO–Al_2O_3 catalyst layer adhered strongly not only at the lateral side but also at the corner of the channel. From this result, it could be known that the SiO_2 layer was able to replace the conventionally used Al_2O_3 adhesion

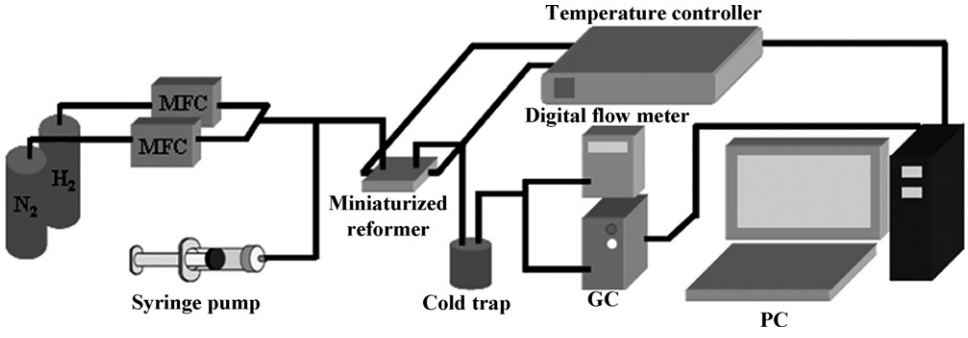

Fig. 3. A schematic diagram of an experimental setup.

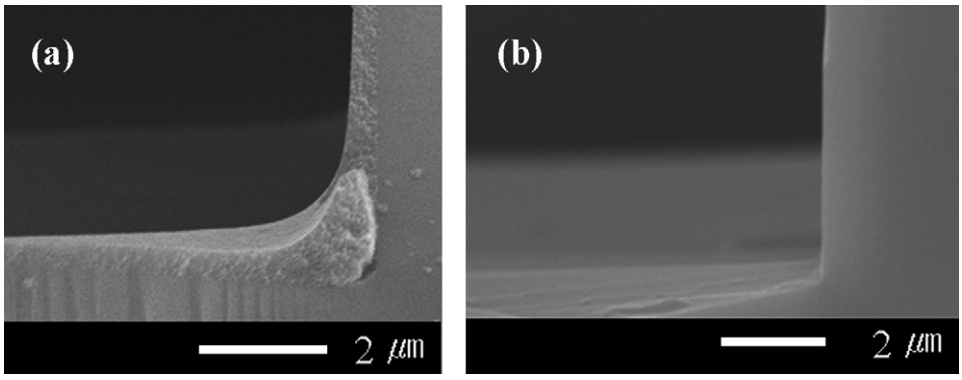

Fig. 4. FESEM images of (a) an Al_2O_3 adhesion layer and (b) a SiO_2 adhesion layer.

layer. Moreover, the SiO_2 layer gave not only simple fabrication process but also more space to cross-sectional area of channel without loosing or reducing the adhesion of Cu–ZnO–Al_2O_3 catalyst layer due to the thin layer thickness. Thus, the SiO_2 layer was introduced instead of the Al_2O_3 layer for all following experiments.

Besides the good adhesion property, a simple fabrication process and a large cross-sectional area, the SiO_2 layer makes it possible to fabricate various design channels, because it does not require air pushing step that has restricted channel design into serpentine channel. Using SiO_2 layer, two types of reformers were fabricated to compare the effect of channel design on the performances of reformers. One was a serpentine channel reformer which had a continuous single channel, and the other was a parallel channel reformer which had four parallel subchannels as shown in Fig. 2. Although both reformers showed different channel design, a channel volume and a coated catalyst weight (20 mg for each reactor) were controlled to be same to make reactants feel same experimental condition in both reformers. The same channel volume and the catalyst weight were necessary to only compare channel design effect. As appearing in Fig. 7, the maximum gas production rates obtained with 10 $cm^3\,h^{-1}$ methanol feed rate were 300 $cm^3\,min^{-1}$ (hydrogen 225 $cm^3\,min^{-1}$) in serpentine channel at 300 °C with 100% conversion, and 243 $cm^3\,min^{-1}$ (hydrogen 182 $cm^3\,min^{-1}$) in parallel channel at 320 °C with 80.2% conversion. Since the gas production rate rose according to both methanol feed rate and operation temperature, 100% conversion in the parallel channel reformer might be achieved over 320 °C. However, due to the deactivation of a catalyst at high temperature, the temperature was limited up to 320 °C in this study.

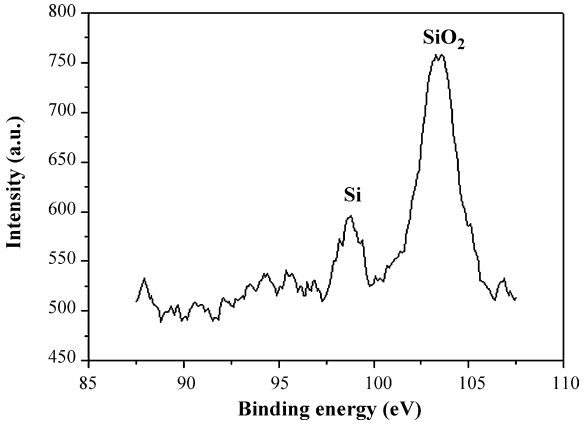

Fig. 5. Angle resolved XPS data of a bare Si substrate obtained in the take-off angle of 90°.

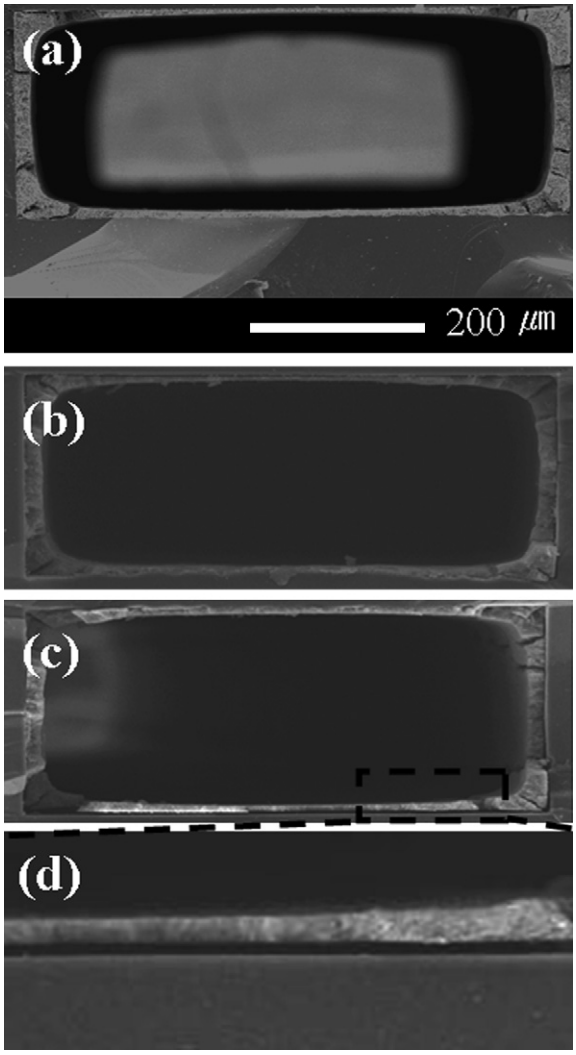

Fig. 6. The FESEM images of catalyst coating profiles (a) with a SiO_2 adhesion layer, (b) with an Al_2O_3 adhesion layer, (c) without an adhesion layer, and (d) enlargement of (c).

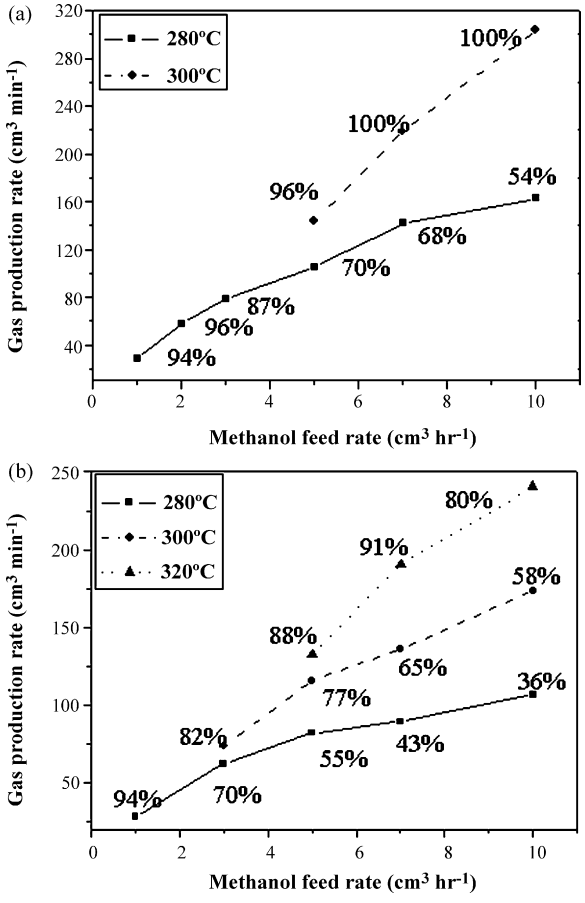

Fig. 7. The gas production rate and the conversion of (a) a serpentine channel reformer and (b) a parallel channel reformer. The % number in the figure means the conversion.

In the gas production rate comparison, the serpentine and the parallel channel reformers gave different performance, in spite of they were designed to have the same channel volume and the catalyst weight. It is thought that this is due to pressure drop difference. The higher pressure drop of the serpentine channel results in that the partial pressures of reactants of the serpentine channel are higher than those of reactants of the parallel channel. Higher partial pressure of reactants enhances the reaction rate of steam reforming of methanol. This is the reason why the serpentine channel reformer showed the higher conversion than the parallel channel reformer at the same channel volume and the catalyst weight condition.

Fig. 8(a) shows the CO concentration of the parallel channel reformer in which vaporizing zone was formed at the front of the reformer without connecting an additional vaporizer as shown in Fig. 8(c). The result of the parallel channel reformer gives different trend in CO concentration variation, when it is compared with the result of the serpentine channel reformer. The CO concentration is proportional to the methanol feed rate in the parallel channel reformer as shown in Fig. 8(a), whereas the CO concentration decreases as methanol feed rate is raised in the case of the serpentine channel reformer [13]. Thus, the parallel channel reformer shows higher CO concentration than the serpentine channel reformer at high methanol feed rate. For example, it is 4000 ppm higher at 10 $cm^3\ h^{-1}$ methanol feed rate.

The vaporization occurring in vaporization region removes heat from a inlet area, leading to a heat flux from the outlet to the inlet. Thus, the temperature drop at the inlet and the temperature elevation at the outlet increases as methanol feed rate is raised. With the increase in a methanol feed, the reverse water gas shift reaction which is an endothermic reaction is more favorable at

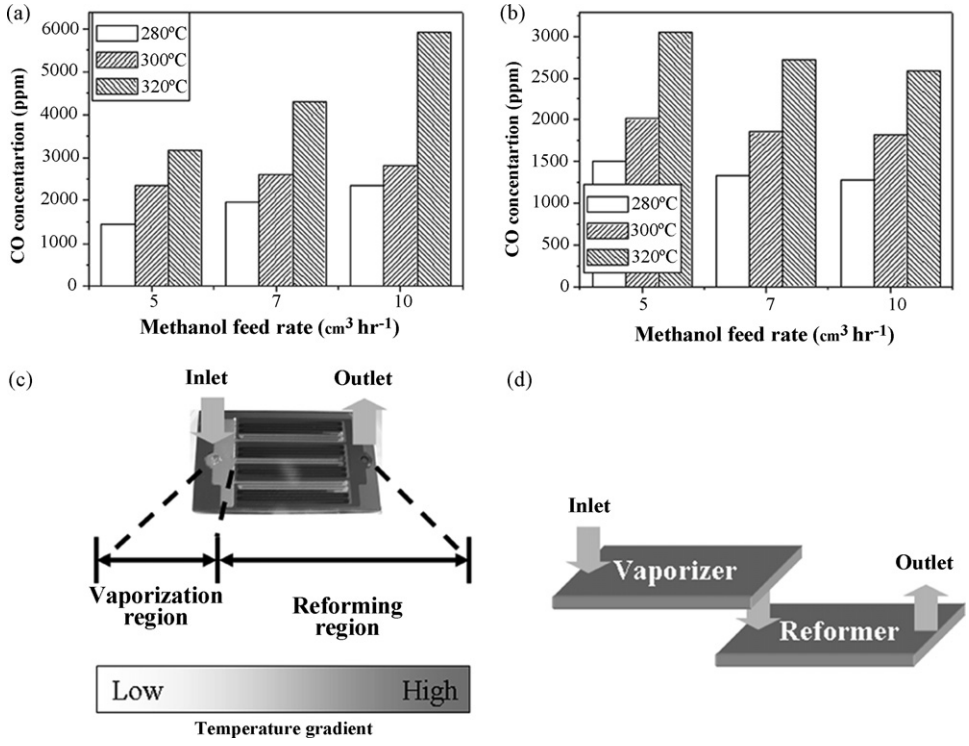

Fig. 8. The CO concentrations of (a) a parallel channel reformer integrated with a vaporizer and (b) an as-prepared parallel channel reformer, and the structure of (c) an as-prepared parallel channel reformer and (d) the schematic diagram of a parallel channel reformer integrated with a vaporizer.

the end of the reforming region than an exothermic water gas shift reaction. This explains why the CO concentration in the parallel channel reformer is proportional to the methanol feed rate at a fixed operation temperature as shown in Fig. 8(a). To certify that temperature gradient was the reason for the high CO concentration at high methanol feed rate, additionally, a separated vaporizer was connected to the parallel channel reformer as show in Fig. 8(d). With the adoption of the separated vaporizer, the concentration of CO decreased according to the methanol feed rate as shown in Fig. 8(b). This result makes sure that the temperature gradient caused by the vaporization of methanol at the vaporization region generates high CO concentration in the parallel channel reformer. The temperature gradient of the parallel channel reformer is caused by the setup which has only one heating element and one thermocouple to control the temperature. Thus, two different heating elements with separated control loops would solve the problem. Although two different heating elements could not be applied to one reformer due to the heat conductivity of the silicon in this experiment, the separated control loops those were introduced by adding the separated vaporizer demonstrate the effect of two different heating elements.

In the comparison of a serpentine channel reformer and a parallel channel reformer, the serpentine channel reformer was superior to the parallel channel reformer in both the conversion and the CO concentration. Nonetheless the parallel channel reformer was more suitable for the scaling up of the reformer, because its hydrogen production rate per unit volume of the reformer was higher than that of the serpentine channel reformer. Parallel channel reformer showed 177 $cm^3\ min^{-1}\ ml^{-1}$ (hydrogen production rate per unit volume). Furthermore, it gave much freedom in designing reformer. Thus, to take these advantages of the parallel channel reformer, the scaling up of reformers was carried out with the parallel channel reformer as shown in Fig. 9. Fig. 9 showed the reformer stack which was made up of six parallel channel reformers. For this experiment, 120 mg of catalyst were used. The stacking of reformer was performed with eutectic bonding and heat resistant silicon. The reformer stack has the volume of 15 cm^{-3} without packaging and 44.8 cm^{-3} with packaging.

The gas production rate and the CO concentration of the reformer stack are shown in Fig. 10. They were monitored varying the methanol feed rate. The gas production rate is proportional to the methanol feed rate, and finally reached the gas production rate of 1054 $cm^3\ min^{-1}$ with the standard deviation of 72 $cm^3\ min^{-1}$. When it is converted into power, it corresponds to 133 W_t (thermal watt), and 75.77 W if a fuel cell has 0.7 V and 100% hydrogen utilization. The superiority of the miniaturized reformer can be proved by comparing the result with the work of Purnama et al. who used the conventional packed bed reformer [17]. When the methanol conversion is compared as a function of the W/F_m ratio (W: mass of the catalyst (kg) and F_m: flow rate of methanol (mmol s^{-1})), the conversion of the miniaturized reformer is higher than Purnama's result that uses a commercial Cu–ZnO–Al_2O_3 (Süd-Chemie) catalyst at same operation conditions (W/F_m ratio, operation temperature, steam to carbon ratio of the methanol solution). For example, the minia-

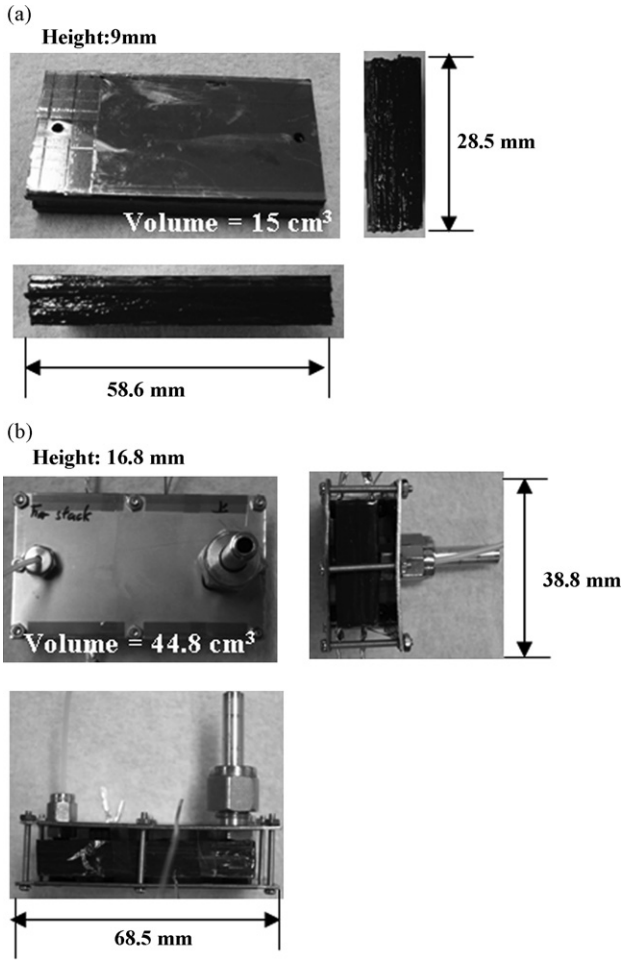

Fig. 9. The photo images of the reformer stack (a) without packaging and (b) with packaging.

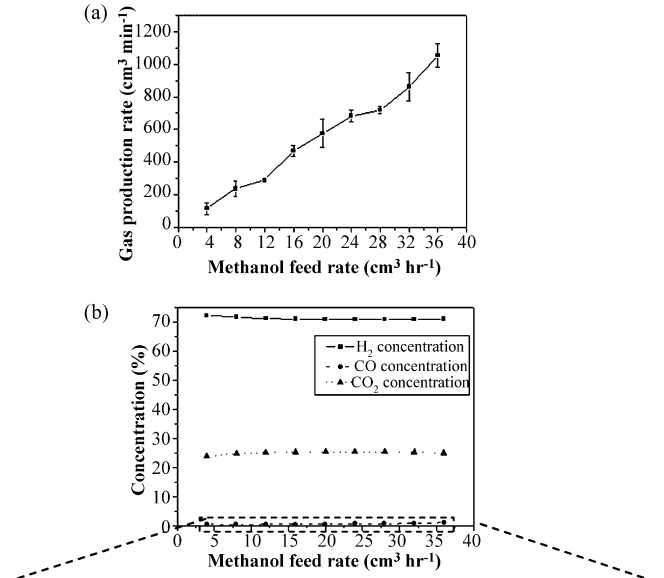

Fee rate (ml/hr)	4	8	12	16	20	24	28	32	36
Concentration (%)	0.5594	0.3935	0.5316	0.5936	0.6173	0.7094	0.7400	0.8929	1.172

Fig. 10. (a) The gas production rate and (b) the CO concentration of a reformer stack.

turized reformer gave 88% conversion whereas the conventional reformer showed around 45% conversion at the W/F_m ratio of 0.00083.

The CO concentration of reformer stack shows same trend with a single parallel channel reformer. The concentration increases according to a methanol feed rate. The highest value of 1.172% was detected at a 36 $cm^3\,h^{-1}$ methanol feed rate. Although it is too high to directly supply for fuel cells, if preferential oxidation reactor is introduced between the reformer stack and fuel cells, this reformer stack is able to be applied for high electrical power notebook computer.

5. Conclusion

A miniaturized reformer was made by a silicon fabrication technology and a fill-and-dry catalyst coating method. Two kinds of adhesion layers of a conventionally used Al_2O_3 layer and a newly introduced SiO_2 layer were tested as the adhesion layers in micro-channels. Both of them showed good adhesion property and demonstrated the similar gas production rate with D.I. water-based catalyst. The SiO_2 layer was applied as an adhesion layer in this study because of its outstanding advantage for designing various channels. With the SiO_2 adhesion layer, the performance of reformer was analyzed with varying channel design from the serpentine to the parallel.

The parallel channel reformer gave better hydrogen production rate than the serpentine channel reformer showing the 177 $cm^3\,min^{-1}\,ml^{-1}$ (hydrogen production rate per unit volume of reformer), even though the CO concentration was higher than the serpentine channel reformer at high methanol feed rate. To take advantage of a high hydrogen production rate of the parallel channel reformer, a reformer stack was made with six parallel channel reformers by stacking them using an eutectic bonding and a heat resistant silicon. It showed the hydrogen production rate of 754 $cm^3\,min^{-1}$ and 1.172% CO concentration. If hydrogen is converted into power, it corresponds to 71 W when a fuel cell has 0.7 V operation potential and 100% conversion, and the power is sufficient for high electrical power notebook computer.

Acknowledgements

This work was supported by KOSEF through the Research Center for Energy Conversion and Storage (RCECS), Seoul Renewable Energy Research Consortium (Seoul RERC) and NIT Share-ISRC Program through Inter-University Semiconductor Research Center (ISRC).

References

[1] J.P. Meyers, H.L. Maynard, J. Power Sources 109 (2002) 76–88.
[2] C. Hebling, A. Heinzel, Fuel Cells Bull. (2002) 8–12.
[3] J.D. Morse, A.F. Jankowski, R.T. Graft, J.P. Heyes, J. Vac. Sci. Technol. A 18 (2000) 2003–2005.
[4] S.C. Kelly, G.A. Deluga, W.H. Smyrl, Electrochem. Solid State Lett. 3 (2000) 407–409.
[5] P. Reuse, A. Renken, K. Haas-Santo, O. Görke, K. Schubert, Chem. Eng. J. 101 (2004) 133–141.
[6] G. Park, D.J. Seo, S. Park, Y. Yoon, C. Kim, W. Yoon, Chem. Eng. J. 101 (2004) 87–92.
[7] L. Pan, S. Wang, Int. J. Hydrog. Energy 30 (2005) 973–979.
[8] A.V. Pattekar, M.V. Kothare, J. Microelectromech. Syst. 13 (2004) 7–18.
[9] K. Haas-Santo, M. Fichtner, K. Schubert, Appl. Catal. A: Gen. 220 (2001) 79–92.
[10] H. Hamatsu, M. Nagase, K. Kurihara, K. Iwadate, K. Murase, Microelectron. Eng. 27 (1995) 71–74.
[11] M.A. Schmidt, Proc. IEEE 86 (1998) 1575–1585.
[12] R.S. Besser, X. Ouyang, H. Surangalikar, Chem. Eng. Sci. 58 (2003) 19–26.
[13] O.J. Kwon, S.M. Hwang, J.G. Ahn, J.J. Kim, J. Power Sources 156 (2006) 253–259.
[14] B.E. Yoldas, Ceram. Bull. 54 (1974) 289.
[15] J.R. Shallenberger, D.A. Cole, S.W. Novak, R.L. Moore, J. Vac. Sci. Technol. B 18 (2000) 440.
[16] S. Wolf, R.H. Tauber, Silicon Processing for the VLSI Era, Lattice Press, 1943, pp. 265–323.
[17] H. Purnama, T. Ressler, R.E. Jentoft, H. Soerijanto, R. Schlogl, R. Schomacker, Appl. Catal. A: Gen. 259 (2004) 83–94.